Materials Science in Semiconductor Processing 147 (2022) 106699

Contents lists available at ScienceDirect

Materials Science in Semiconductor Processing

journal homepage: www.elsevier.com/locate/mssp

Preparation of TiO_2–MoO_3 composite nanofibers by water-based electrospinning process and their application in photocatalysis

Vincent Otieno Odhiambo [a,*], Thong Le Ba [a], Zoltán Kónya [b], Csaba Cserháti [c], Zoltán Erdélyi [c], Maritim C Naomi [d], Imre Miklós Szilágyi [a,**]

[a] Budapest University of Technology and Economics, Department of Inorganic and Analytical Chemistry, H-1111, Budapest, Szent Gellért tér 4., Hungary
[b] University of Szeged, Department of Applied and Environmental Chemistry, H-6720, Szeged, Rerrich Béla tér 1., Hungary
[c] University of Debrecen, Faculty of Sciences and Technology, Department of Solid State Physics, H-4026, Debrecen, Bem tér 18/b., Hungary
[d] University of Pannonia, Department of Analytical Chemistry, Egyetem. út 10., Veszprém, 8200, Hungary

ARTICLE INFO

Keywords:
Electrospinning
Visible light TiO_2–MoO_3 nanofibers
Photocatalysis

ABSTRACT

Coupling TiO_2 nanofibers with other semiconductor metal oxides can effectively extend the light absorbability of TiO_2 to the visible range of the electromagnetic spectrum. This study demonstrates the synthesis of TiO_2–MoO_3 composite nanofibers via electrospinning using Ti and Mo water-soluble precursors. Aqueous solutions of these precursors were added to a PVP solution in N–N dimethylformamide. The mixture was electrospun, followed by annealing in air at 600 °C obtaining oxide nanofibers. The fibers were characterized via thermogravimetry and differential thermal analysis, X-ray photoelectron spectroscopy, scanning electron microscopy and energy-dispersive X-ray spectroscopy, transmission electron microscopy, Fourier-transform infrared spectroscopy, X-ray diffraction, and Raman spectroscopy. The diameter of the TiO_2–MoO_3 fibers was between 90 and 110 nm after annealing, Furthermore, methylene blue dye was used to investigate the photocatalytic activity of the fibers in visible light. TiO_2–MoO_3 fibers showed the best photocalaytic activity with a rate constant of 0.0018 min^{-1} while pure TiO_2 and MoO_3 nanofibers had 0.0009 min^{-1} and 0.0008 min^{-1} respectively.

1. Introduction

Several studies have been conducted on the application of semiconductor oxides to address the challenges of environmental pollution caused by emissions of hazardous industrial wastes [1–4]. Reactions involving the use of TiO_2-based photocatalysts are some of the most extensively investigated methods of controlling environmental pollution. This can be attributed to the high photoreactivity and low cost of TiO_2 [5–8]. When TiO_2 absorbs ultraviolet (UV) light, electrons are excited from the valence band to the conduction band, this leads to formation of holes in the valence band (h^+_{vb}) and electrons in the conduction band (e^-_{cb}). The photogenerated electron–hole pairs might migrate to the surface and combine with air and water molecules to form very reactive hydroxyl radicals (OH*) and superoxide anions (O_2^-). These radicals and anions initiate redox processes that degrade organic and inorganic compounds [9,10]. The mechanism for photocatalysis is shown in Fig. 1.

The major limitation of TiO_2 is that it absorbs only UV light and the electron–hole pairs recombine quickly [12–14]. Conversely, the visible light activation of TiO_2 significantly improves its photocatalytic activity, achieved by doping it with other semiconductor oxides, metals, and non metals [15,16]. Studies have shown that composite semiconductor nanostructures possess integrated multiple functionalities of their constituent materials, making them attractive for application in many fields [17]. Among the semiconductors that can be combined with TiO_2 is MoO_3, an n-type semiconductor with unique properties that enhance its application in many fields, including photochromic and electrochromic applications, energy storage, and photocatalysis [18]. Coupling TiO_2 with MoO_3 can lead to visible light absorption and increase available oxygen valencies as well as life span of the photoexcited electron–hole pairs [19,20].

Elder et al. synthesized nanocrystalline TiO_2–MoO_3 core-shell

* Corresponding author.
** Corresponding author.
E-mail addresses: votieno2000@yahoo.com (V.O. Odhiambo), kenty9x@gmail.com (T. Le Ba), konya@chem.u-szeged.hu (Z. Kónya), cserhati.csaba@science.unideb.hu (C. Cserháti), zoltan.erdelyi@science.unideb.hu (Z. Erdélyi), naomimaritim@gmail.com (M. C Naomi), szilagyi.imre.miklos@vbk.bme.hu (I. Miklós Szilágyi).

https://doi.org/10.1016/j.mssp.2022.106699
Received 7 October 2021; Received in revised form 5 February 2022; Accepted 4 April 2022
Available online 29 April 2022

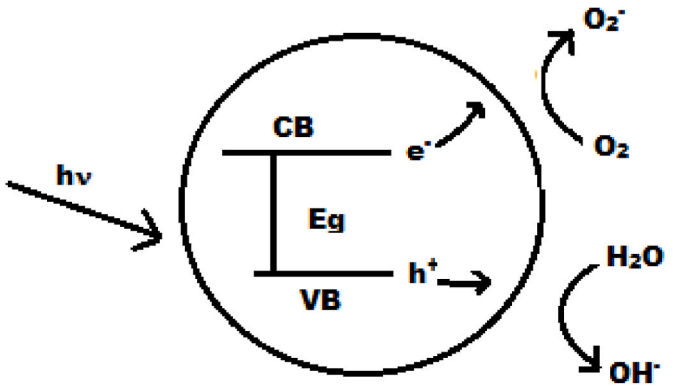

Fig. 1. Mechanism for photocatalysis [11].

materials by co-nucleating metal oxide clusters on surfactant micelles for solar energy conversion. The materials demonstrated a significant decrease in energy bandgap to 2.60 eV [21]. Tatsuma et al. synthesized TiO_2–MoO_3 films via spin coating techniques. They reported that the films could be used as energy storage photocatalysts and antibacterial materials in humid conditions [22]. Kobayashi et al. fabricated TiO_2/-MoO_3 films using the Langmuir–Blodgett technique. The films photocatalytically decomposed stearic acid in visible light [23]. Shouli et al. prepared composite TiO_2/MoO_3 by sol-gel method to improve the phototcalytic performance of TiO_2 under visible light. They reported that the composite substance degraded Rhodamine B dye faster than pure TiO_2 invisible light [24]. They attributed the improved photocatalytic activity to the formation of heterostructures hence reduction in the rate of charge recombination. Zhu et al. used hydrothermal synthesis to prepare composite TiO_2 nanobelts/MoO_3 nanosheets for enhanced solar driven phototcatalysis. They used TiO_2–MoS_2 as precursors. TiO_2/MoO_3 composite heterostructures had better phototcatalytic activity than the pure TiO_2 nanobelts and MoO_3 nanosheets [25].

Pure TiO_2 and MoO_3 nanofibers have been synthesized by electrospinning [26,27]. However, there are no reports on preparation of TiO_2–MoO_3 composite nanofibers by electrospinning using water-soluble precursors. while ammonium molybdate tetrahydrate (AMT) is water soluble, most TiO_2 precursors are insoluble in water. Furthermore, AMT is insoluble in ethanol, a solvent commonly used to dissolve most polymers used in electrospinning. The novelty of this work is the development of a simple method for preparation of TiO_2–MoO_3 composite nanofibers using a water-based electrospinning process. In electrospinning, fibers are synthesized by drawing polymer solutions from a needle tip using high voltage and then depositing them on a grounded collector [28,29].

TiO_2–MoO_3 nanofibers were prepared in this study by electrospinning and annealing in air. Water-soluble titanium (IV) bis (ammonium lactato) dihydroxide (TiBALDH) and AMT were used as precursors for TiO_2 and MoO_3, respectively, while N–N dimethylformamide (DMF) was used to prepare the polymer solution. The electrospun fibers were annealed in air. The resulting fibers were investigated by thermogravimetry and differential thermal analysis (TG/DTA), X-ray photoelectron spectroscopy (XPS), scanning electron microscopy and energy-dispersive X-ray (SEM–EDX) spectroscopy, transmission electron microscopy (TEM), Fourier-transform infrared (FTIR) spectroscopy, X-ray diffraction (XRD), Raman and UV–Vis spectroscopy. Moreover, methylene blue dye was used to establish the photocatalytic activity of the fibers in visible light.

2. Materials

Polyvinylpyrrolidone [PVP, $(C_6H_9NO)_n$, K-90], TiBALDH, AMT, and DMF were obtained from Sigma-Aldrich and used as received. The percentage purity of the materials was 99.9% and the molecular weight for PVP was 90,000.

2.1. Preparation of TiO_2–MoO_3 nanofibers

An aqueous solution of AMT containing 1 g of AMT in 3 mL of distilled water was mixed with different volumes of TiBALDH to obtain a mixture with varying volume ratios of 100%, 50%, and 0%. Next, 2 mL of this mixture was added to 2 mL of 20% PVP solution in DMF. The mixture was stirred overnight at 25 °C before electrospinning using a voltage of 20 kV and a flow rate of 1 mLh^{-1}. The distance between the needle tip and aluminum foil screen that was covered by a polyethylene sheet was 12 cm.

2.2. Characterization of the nanofibers

The thermal properties of the electrospun fibers were determined in an STD 2960 Simultaneous TG/DTA (TA Instruments Inc.) thermal analyzer. The samples were heated in air at 10 °C min^{-1} up to 600 °C. The morphology and composition of the oxide fibers were investigated using XPS, SEM–EDX, and TEM. XPS spectra were determined using a SPECS XPS instrument fitted with an XR-50 dual anode X-ray source and a Phoibos 150 energy analyzer. The powdered samples were pressed onto an Indium (In) foil for mounting. The Al Kα X-ray source with 150 W (14 kV) was employed for the measurements. The survey spectra were obtained with a step size of 1 eV and pass energy of 40 eV. High-resolution spectra were acquired with a step size of 0.1 eV and a pass energy of 20 eV with 25 scans. JEOL JSM-5500LV SEM was used to perform the SEM–EDX analysis. The TEM images of the annealed fibers were obtained using JEOL 200 FX-II TEM. The fibers were sonicated in ethanol for 10 min after which the liquids containing the fibers were dropped onto a TEM grid covered with carbon.

Attenuated total reflection FTIR (ATR-FTIR) measurements of electrospun and annealed nanofibers were performed using a Bruker Tensor 37 fitted with a Specac Golden Gate ATR accessory.

A PANalytical X'pert Pro MPD XRD apparatus was used to determine the XRD patterns of the annealed fibers by Cu K_α irradiation. Raman spectra were obtained from an Olympus BX41 microscope fitted Jobin Yvon Labram Raman instrument within a range of 72–1560 cm^{-1}. UV–Vis diffuse reflectance spectra of the annealed fibers were obtained measured using Avaspec 2048 with fibre optic spectrophotometer between 250 nm and 800 nm.

2.3. Photocatalysis

Methylene blue indicator was used to investigate the photocatalytic activity of the fibers in visible light. First, 1.0 mg of the annealed fibers was added to a 3-ml aqueous solution of methylene blue dye at a concentration of 0.0126 g/L in a quartz cuvette. The samples were left in a dark room for 12 h to establish adsorption equilibrium and then exposed to visible light lamps. The decomposition of the methylene blue was assessed by measuring its absorbance at 664 nm every half hour with a Jasco V-550 UV-VIS spectroscope for 4 h [30].

3. Results and discussion

The TG/DTA curves obtained during the annealing of the fibers in air are shown in Fig. 2 a-c. Based on the curves, the decomposition of the fibers was continuous and showed similar patterns. The small loss in mass, about 7% before reaching a temperature of 100 °C, can be attributed to the loss of adsorbed water particles from the fibers. The change in mass between 300 °C and 550 °C accompanied by the exothermic peaks in the DTA can be attributed to the combustion of the polymer component of the fibers and the decomposition of the precursors, resulting in the formation of the corresponding oxides. The peak around 310 °C in the DTA corresponds to the combustion process of the polymer. In the decomposition step between 400 °C and 550 °C, the salt

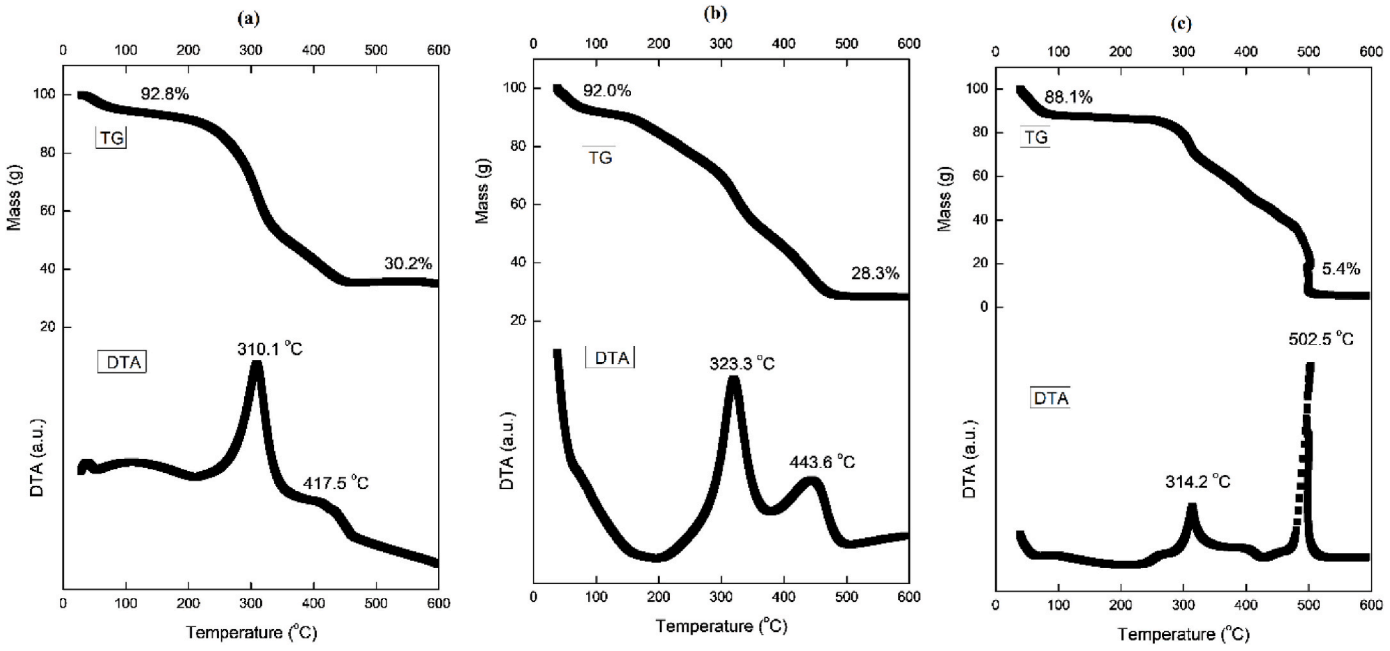

Fig. 2. TG/DTA curves (a) TiO_2 (b) TiO_2–MoO_3 and (c) MoO_3.

precursors decomposed and PVP carbon residues were combusted. Similar decomposition phenomena have been reported in other studies [31,32]. No change was observed in the fibers beyond 600 °C from the TG curves. Therefore, the fibers were annealed in the furnace until 600 °C.

Figs. 3 and 4 show the XPS spectra of the fibers after annealing in air. Fig. 3 shows the survey spectra of the fibers. Pure TiO_2 demonstrated O 1s, Ti 2p, and C 1s peaks, with O 1s and Ti 2p being the most intense, while MoO_3 exhibited O 1s, Mo 3d, and C 1s peaks. The composite fibers showed peaks for TiO_2 and MoO_3. The presence of C 1s peaks was attributed to the presence of adventitious carbon on the fiber surface. The presence of In in the spectrum is explained by the In foil that was used in the measurements.

Fig. 4 shows the Ti 2p XPS spectra for pure and composite fibers. The Ti $2p_{1/2}$ peak was observed at 464.2 eV, whereas the Ti $2p_{3/2}$ peak was observed at 458.6 eV. This was consistent with Ti^{4+} in TiO_2 lattice. In the composite fibers, the $Ti_{2P3/2}$ peak at 457.0 eV was assigned to Ti^{3+}

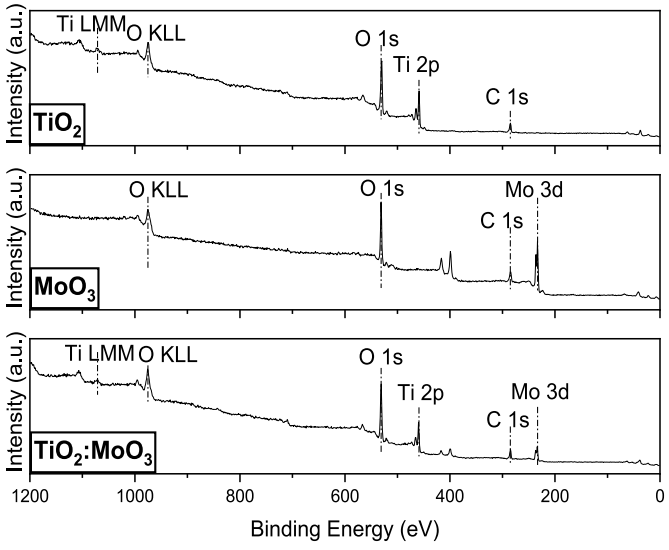

Fig. 3. XPS survey spectra of TiO_2, MoO_3, and TiO_2–MoO_3 fibers.

[33]. The deconvoluted Mo 3d spectra indicated that the fibers contained Mo^{6+} and Mo^{5+}. Mo $3d_{5/2}$ and Mo $3d_{3/2}$ peaks at 233.0 and 236.1 eV, respectively, are consistent with Mo^{6+}. Peaks at 231.8 and 234.9 eV were assigned to Mo^{5+} $3d_{5/2}$ and Mo^{5+} $3d_{3/2}$, respectively [34]. A small shift of 0.5 eV was observed in the binding energy associated with Mo^{6+}.

The morphologies of TiO_2, MoO_3, and TiO_2–MoO_3 fibers are demonstrated by SEM and TEM images in Fig. 5, while Table 1 shows the fiber diameter and results of EDX analysis of the annealed fibers. The analysis revealed that the samples were fibrous and exhibited smooth surfaces and long lengths. Due to the degradation of the polymer component of the fibers and decomposition of the precursors, the diameter of the samples decreased after annealing. The EDX analysis of the annealed fibers confirmed the presence of Ti and Mo in the composite fibers, where the ratio of TiO_2 to MoO_3 exceeded 1:1, which can be attributed to the higher solubility of TiBALDH in water than in AMT.

Fig. 6 shows the FTIR spectra of as-spun and annealed fibers. The as-spun fibers showed peaks attributed to the functional groups in the polymers and precursors. The broad peaks around 3500 cm^{-1} can be attributed to the O–H stretching vibrations, while peaks around 3150 cm^{-1} were due to NH_4^+ stretching vibrations. Furthermore, C═O and C–OH stretching vibrations were observed around 1650 cm^{-1} and 1200 cm^{-1}, respectively. The annealing process decomposed the polymer and degraded the precursors resulting in the absence of peaks in the annealed fibers. Mo═O stretching vibrations were observed around 1060 cm^{-1}, while the band around 820 cm^{-1} is associated with vibrations of O atoms in MoO_3 lattice [35,36]. The peak around 600 cm^{-1} was assigned to Ti–O vibrations [37]. The FTIR spectra demonstrated that the annealing process successfully decomposed the polymer component of the fibers and degraded the precursors to form TiO_2, TiO_2–MoO_3, and MoO_3 fibers.

Fig. 7 shows the XRD patterns of the annealed fibers. MoO_3 exhibited diffraction peaks characteristic of orthorhombic MoO_3 at 12.7°, 23.5°, 26.0°, 27.4°, 33.8°, 34.0°, 39.1°, 46.2°, 46.5°, and 49.5° assigned respectively to (020), (110), (040), (021), (101), (111), (060) (200), (210), and (002) planes [38]. The patterns were indexed to ICDD 01-075-0912. TiO_2 fibers had strong diffraction peaks for anatase TiO_2 at 25.5°, 38.1°, 48.4°, 54.0°, 55.2°, and 62.9° corresponding to (101), (004), (200), (105), (211), and (204) planes [39]. The diffraction patterns were indexed to ICDD 04-016-2837. TiO_2–MoO_3 fibers showed

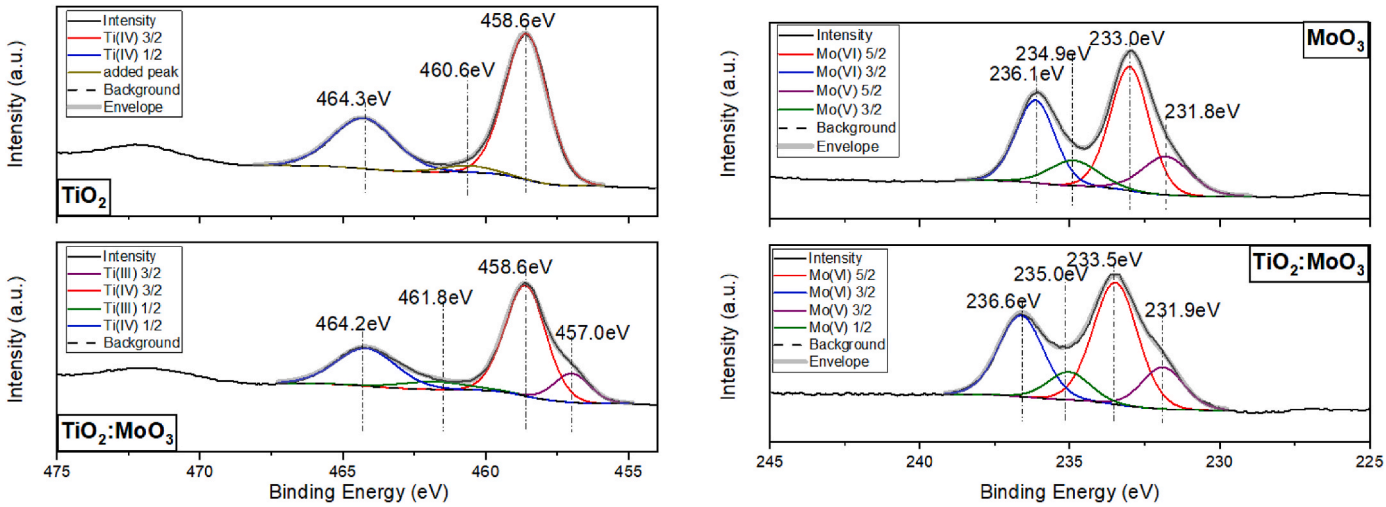

Fig. 4. Ti 2p and Mo 3d XPS spectra for TiO_2, MoO_3, and TiO_2–MoO_3 fiber.

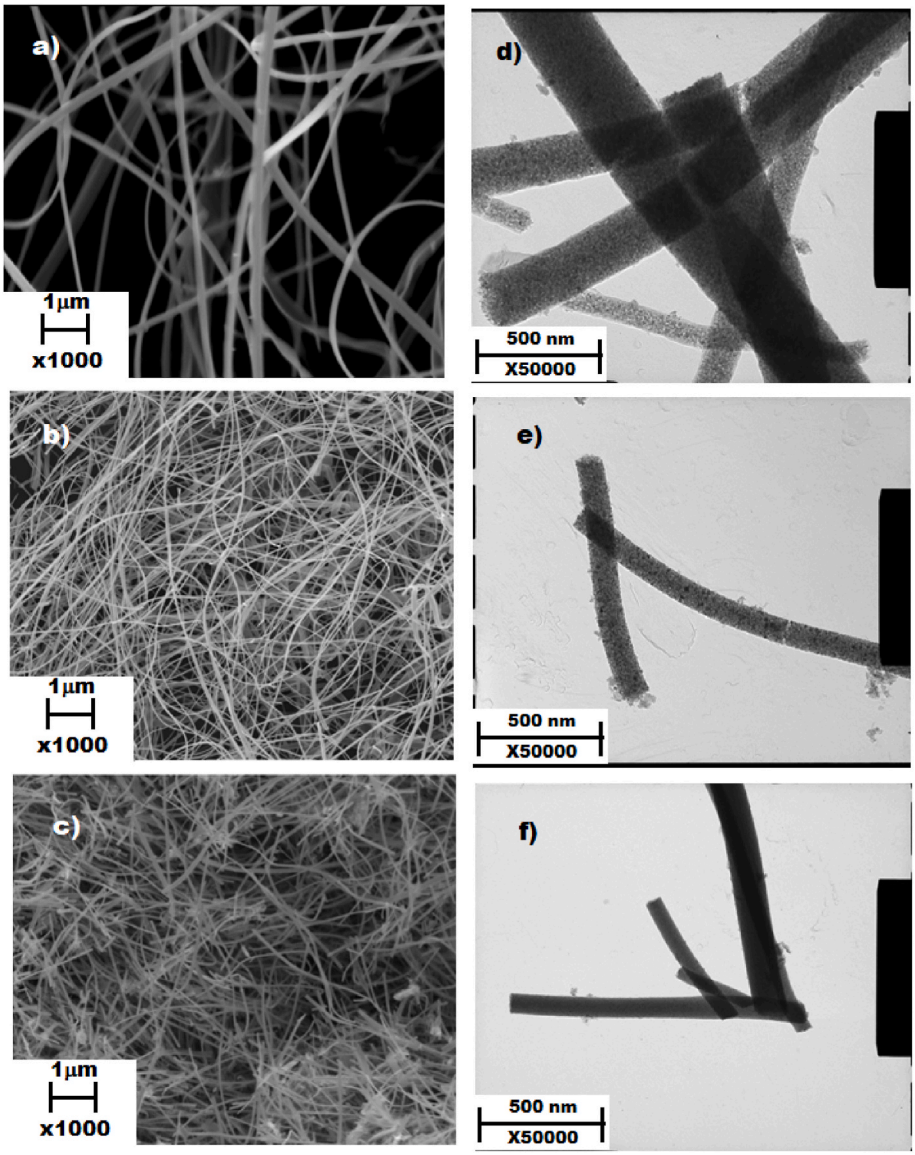

Fig. 5. SEM and TEM images of annealed fibers: a) SEM TiO_2, b) SEM TiO_2–MoO_3, c) SEM MoO_3, d) TEM TiO_2, e) TEM TiO_2–MoO_3, and f) TEM MoO_3.

Table 1
Fiber diameter and elemental composition of the annealed fiber.

	Fiber diameter (nm)		Elemental composition (at wt%)		
	Before annealing	After annealing	Ti	Mo	O
TiO_2	600–800	90–200	34.1	–	65.9
TiO_2–MoO_3	400–650	70–110	19.5	13.1	67.4
MoO_3	150–300	20–50		29.2	70.8

peaks belonging to both anatase TiO_2 and orthorhombic MoO_3.

Raman spectra of the annealed fibers are shown in Fig. 8. The TiO_2 fibers exhibited Raman active modes, $2E_g$ (144 cm^{-1} and 640 cm^{-1}) and B_{1g} (400 cm^{-1}) and A_{1g} (509 cm^{-1}) characteristic of anatase TiO_2 [40]. MoO_3 exhibited Raman active modes characteristic of the orthorhombic form of MoO_3. The peaks at 288 and 666 cm^{-1} are associated with the Mo═O bending vibration modes, while the peaks at 817 and 994 cm^{-1} are attributed to Mo–O stretching vibrations [41]. Raman active modes of anatase TiO_2 and orthorhombic MoO_3 were observed in the composite fiber.

The optical property of the fibers was investigated using UV–Vis spectroscopy. Fig. 9 presents the diffuse reflectance UV–Vis spectra. The spectra shows that light absorption edge of MoO_3 fibers is above 550 nm. Combining TiO_2 with MoO_3 shifts the light absorption range of the fibers to the visible region of the electromagnetic spectrum. This improves the phototcatalytic activity of TiO_2.

Fig. 10 shows the photocatalytic decay of methylene blue by the fibers in visible light. In the blank set up, there was no degradation of methylene blue within the first 2 h unlike the set ups that contained the fibres and P25 TiO_2. After 4 h the percentage dye degradation was 33, 23, 19 and 17% respectively in TiO_2–MoO_3, P25 TiO_2, TiO_2 and MoO_3 nanofibers. This shows that coupling TiO_2 with MoO_3 significantly increases its phototcatlytic activity. In this study, a p-type semiconductor, TiO_2, is coupled with an n-type semiconductor oxide, MoO_3, by electrospinning. This creates a p–n junction, which promotes the direct transfer of photoexcited electrons from the valence band of TiO_2 to the conduction band of MoO_3. In addition the heterostructure of comoposite nanofibre promotes separation of the active charge carriers leading to improved photocatalytic activity [42]. Furthermore the reusability of the TiO_2–MoO_3 was investigated by carrying out three successive cycles of the degradation process. After each cycle, the composite fibers were washed, fresh MB dye added and the absorbance of the mixture measured at 664 nm every half hour. The activity of the fibres decreased by just 3% after the third cycle, this confirmed the reusability of the composite fibres in phototcatalysis.

The photocatalytic activity follows a pseudo first order kinetic model and the gradient of plot of -ln(relative absorbance) against irradiation time gave the reaction rate constant [43,44]. Table 2 shows the rate constants of the catalytic reactions. The table shows that the activity of TiO_2–MoO_3 is twice that of pure TiO_2 and MoO_3. Similarly, Kobayashi et al. reported that the TiO_2–MoO_3 films synthesized using the Langmuir–Blodgett technique photocatalytically degraded stearic acid at a higher rate than pure TiO_2 films [23].

The rate constant of the photocatalytic reaction of TiO_2–MoO_3

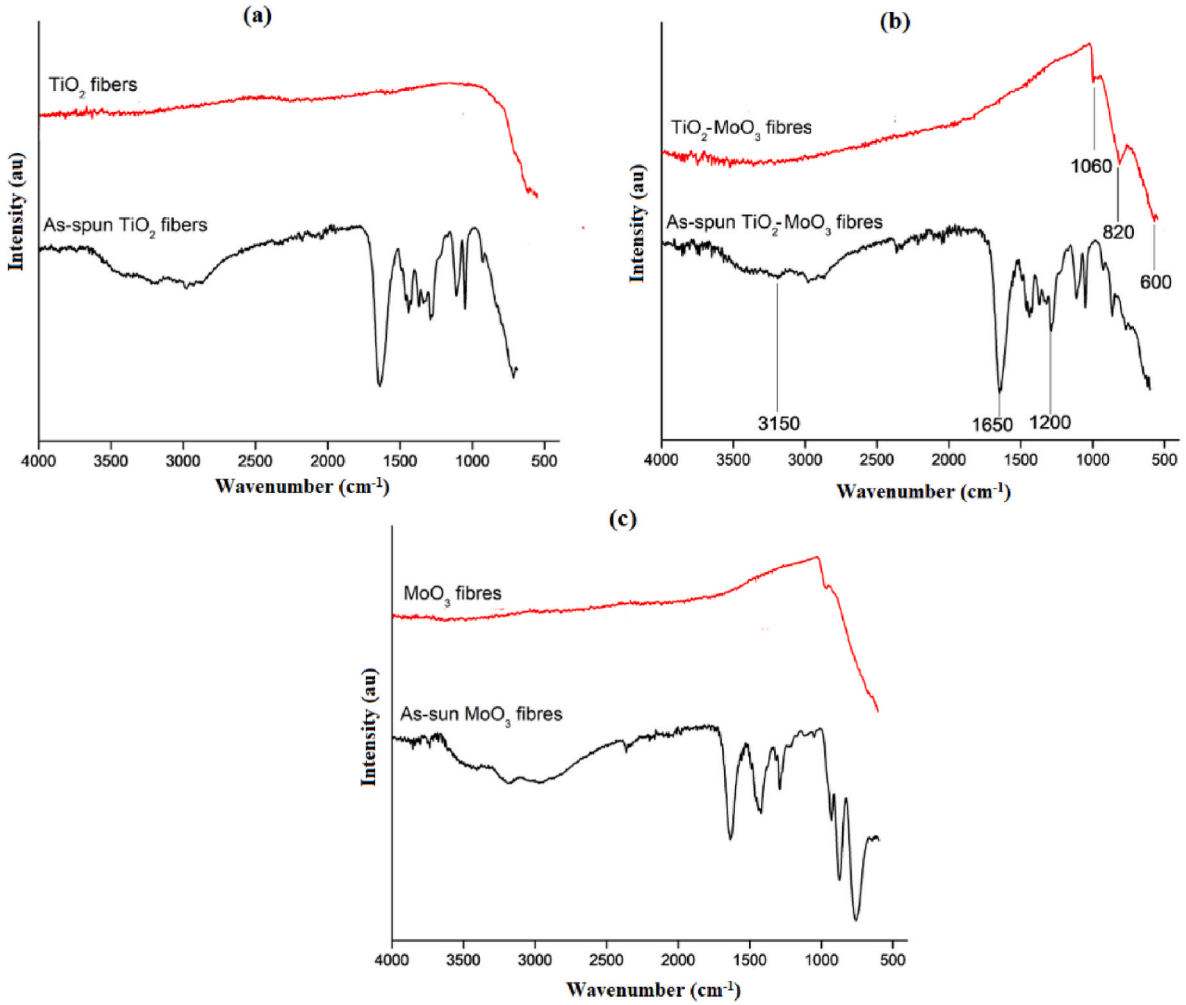

Fig. 6. FTIR spectra of as-spun and annealed fibers: a) TiO_2, b)TiO_2–MoO_3 and c) MoO_3.

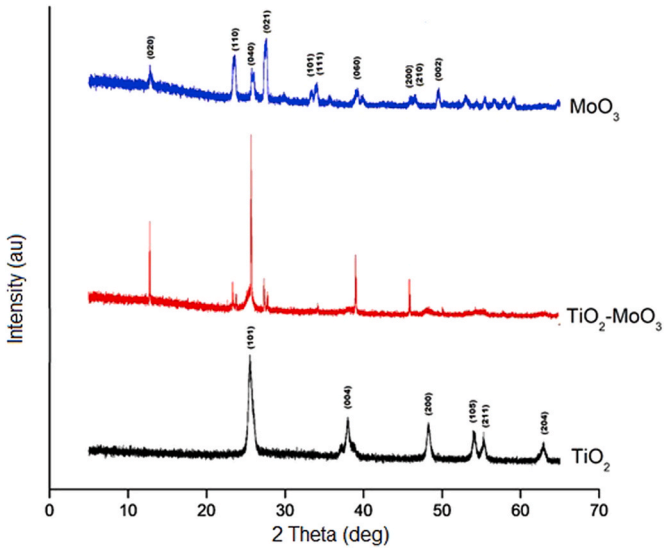

Fig. 7. XRD diffraction peaks of the annealed fibers.

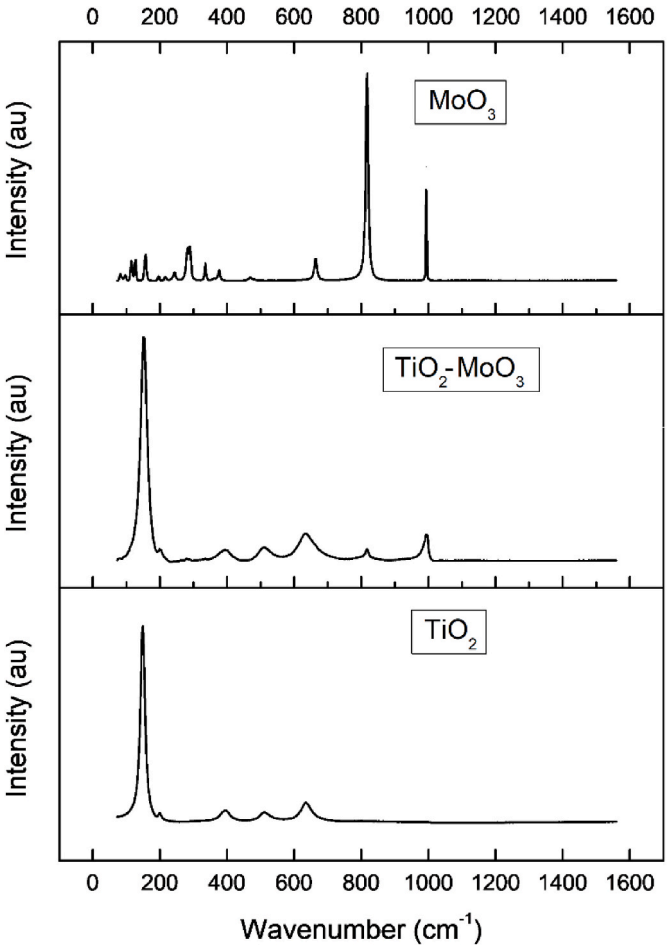

Fig. 8. Raman spectra of annealed fibers.

nanofibers prepared by electrospinning was compared with other TiO_2/MoO_3 heterostructures synthesized by different methods as shown in Table 3. The results show that the rate of phototcatalytic activity of the composite TiO_2–MoO_3 nanofibers prepared by electrospinning is lower than for nanosheets prepared by hydrothermal synthesis but closer to composite heterostructures prepared by sol-gel synthesis.

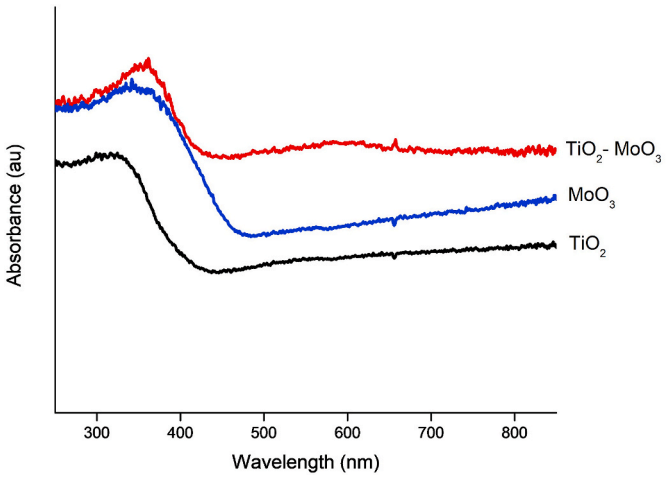

Fig. 9. UV–Vis diffuse reflectance spectra of the annealed fibers.

4. Conclusions

Composite TiO_2–MoO_3 nanofibers were successfully synthesized via a simple and versatile process. Using a water-soluble TiO_2 precursor and DMF as the polymer solvent provided a route for preparing TiO_2–MoO_3 nanofibers via electrospinning for various applications. The characterization of the annealed fibers using XPS, XRD, and Raman techniques confirmed the presence of anatase TiO_2 and orthorhombic MoO_3. DRS UV–Vis spectroscopy showed that light absorption range of TiO_2 was increased by combining it with MoO_3. The composite fibers significantly outperformed the pure fibers and P25 TiO_2 in terms of photocatalytic activity during methylene blue degradation in visible light. Coupling TiO_2 with MoO_3 decreases the rate of recombination of charge carriers during photocatalysis. This improves the photocatalytic activity of TiO_2. The synthesis route employed in this study allows for the fabrication of TiO_2–MoO_3-based nanofibers for various applications.

Funding

An NRDI K 124212 and an NRDI TNN_16 123631 grants are acknowledged. The research within project No. VEKOP-2.3.2-16-2017-00013 was supported by the European Union and the State of Hungary, co-financed by the European Regional Development Fund. The research reported in this paper and carried out at BME has been supported by Stipendium Hungaricum scholarship and the NRDI Fund TKP2021 BME-NVA based on the charter of bolster issued by the NRDI Office under the auspices of the Ministry for Innovation and Technology. .This research is under Project no. TKP2021-NKTA-34 implemented with the support provided from the National Research, Development and Innovation Fund of Hungary, financed under the TKP2021-NKTA funding scheme.

CRediT authorship contribution statement

Thong Le Ba: Writing – review & editing, Methodology. **Zoltán Kónya:** Writing – review & editing, Investigation, Funding acquisition. **Csaba Cserháti:** Writing – review & editing, Investigation. **Zoltán Erdélyi:** Writing – review & editing, Investigation. **Maritim C Naomi:** Writing – review & editing, Investigation. **Imre Miklós Szilágyi:** Writing – review & editing, Supervision, Resources, Methodology, Funding acquisition, Conceptualization.

Declaration of competing interest

The authors declare that they have no known competing financial interests or personal relationships that could have appeared to influence

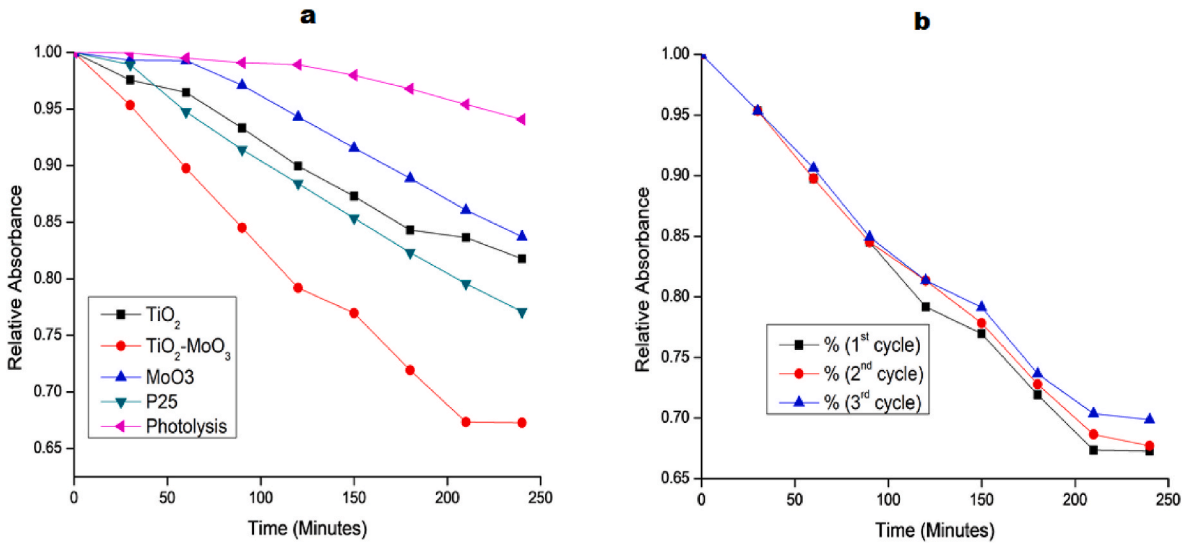

Fig. 10. a) Photocatalytic degradation of methylene blue in visible light b) reusability of TiO_2–MoO_3 composite fibers in degradation of MB in visible light.

Table 2
Rate constant and r^2 values for the photocatalytic activity of the fibers in visible light.

Sample	k_{app} (min^{-1})	r^2
TiO_2	0.0009	0.986
TiO_2–MoO_3	0.0018	0.988
MoO_3	0.0008	0.954
P25	0.0008	0.954
Bare methylene blue	0.0003	0.896

Table 3
Rate constant and r^2 values for photocatalytic activity of different TiO_2–MoO_3 composite heterostructures in visible light.

Photocatalyst	Method of preparation	k_{app} (min^{-1})	r^2	authors
TiO_2–MoO_3 nanofibers	Electrospinning	0.0018	0.988	
TiO_2/MoO_3	sol-gel	0.0027	0.955	Shouli et al. [24]
TiO_2/MoO_3 nanosheets	Hydrothermal	0.00985	0.99	Zhou et al. [25]

the work reported in this paper.

References

[1] A.I. Gopalan, J.C. Lee, G. Saianand, K.P. Lee, P. Sonar, R. Dharmarajan, Y.L. Hou, K.Y. Ann, V. Kannan, W.J. Kim, Recent progress in the abatement of hazardous pollutants using photocatalytic TiO_2-Based building materials, Nanomaterials vol. 10 (2020) 1–50.

[2] I.S. Yunus, Harwin, A. Kurniawan, D. Adityawarman, A. Indarto, Nanotechnologies in water and air pollution treatment, Environ. Technol. Rev. 1 (2012) 136–148.

[3] Y. Li, J. Yan, Q. Su, E. Xie, W. Lan, Materials Science in Semiconductor Processing Preparation of Graphene – TiO_2 nanotubes/nanofibers composites as an enhanced visible light photocatalyst using a hybrid synthetic strategy, Mater. Sci. Semicond. Process. 27 (2014) 695–701.

[4] K.V. Karthik, A.V. Raghu, K.R. Reddy, R. Ravishankar, M. Sangeeta, N.P. Shetti, C. V. Reddy, Green synthesis of Cu-Doped ZnO nanoparticles and its application for the photocatalytic degradation of hazardous organic pollutants, Chemosphere vol. 287 (2022), 132081.

[5] R. Daghrir, P. Drogui, D. Robert, Modified TiO_2 for environmental photocatalytic applications: a review, Ind. Eng. Chem. Res. 52 (2013) 3581–3599.

[6] H. Xu, S. Ouyang, L. Liu, P. Reunchan, N. Umezawa, J. Ye, Recent advances in TiO2-based photocatalysis, J. Mater. Chem. A 2 (2014) 12642–12661.

[7] J. Schneider, M. Matsuoka, M. Takeuchi, J. Zhang, Y. Horiuchi, M. Anpo, D. W. Bahnemann, Understanding TiO2 photocatalysis mechanisms and materials, Chem. Rev. 114 (2014) 9919–9986.

[8] H. Lian, Z. Meng, Materials Science in Semiconductor Processing A novel and highly photocatalytic " TiO_2 wallpaper " made of electrospun TiO_2/bioglass hybrid nano fiber, 80, 2018, pp. 68–73.

[9] V. Etacheri, C. Di Valentin, J. Schneider, D. Bahnemann, S.C. Pillai, Visible-light activation of TiO_2 photocatalysts: advances in theory and experiments, J. Photochem. Photobiol. C Photochem. Rev. 25 (2015) 1–29.

[10] K. Karthik, S. Vijayalakshmi, A. Phuruangrat, V. Revathi, U. Verma, Multifunctional applications of microwave-assisted biogenic TiO_2 nanoparticles, J. Cluster Sci. 30 (2019) 965–972.

[11] Ismaya E.P. Nasikhudin, M. Diantoro, A. Kusumaatmaja, K. Triyana, Preparation of PVA/TiO_2 composites nanofibers by using electrospinning method for photocatalytic degradation, IOP Conf. Ser. Mater. Sci. Eng. 202 (2017), 012011.

[12] N. Justh, L.P. Bakos, K. Hernádi, G. Kiss, B. Réti, Photocatalytic Hollow TiO_2 and ZnO Nanospheres Prepared by Atomic Layer Deposition, 2017, pp. 2–10.

[13] T. Choi, J.S. Kim, J.H. Kim, Transparent nitrogen doped TiO_2/WO_3 composite films for self-cleaning glass applications with improved photodegradation activity, Adv. Powder Technol. 27 (2016) 347–353.

[14] T. Beyza, A. Demi, S. Dursun, I. Keri, I.C. Kaya, V. Kalem, H. Akyildiz, Materials Science in Semiconductor Processing Hydrothermal/Electrospinning Synthesis of CuO Plate-like Particles/TiO_2 Fibers Heterostructures for High-Efficiency Photocatalytic Degradation of Organic Dyes and Phenolic Pollutants, vol. 109, 2020.

[15] P. Chakornpradit, M. Phiriyawirut, V. Meeyoo, Preparation of TiO_2/WO_3 composite nanofibers by electrospinning, Key Eng. Mater. 751 (2017) 296–301.

[16] R. Liu, H. Ye, X. Xiong, H. Liu, Fabrication of TiO_2/ZnO composite nanofibers by electrospinning and their photocatalytic property, Mater. Chem. Phys. 121 (2010), 432–9.

[17] M. Jonnalagadda, V.B. Prasad, A.V. Raghu, Synthesis of composite nanopowder through Mn doped ZnS-CdS systems and its structural, optical properties, J. Mol. Struct. 1230 (2021), 129875.

[18] A. Chithambararaj, A.C. Bose, Hydrothermal synthesis of hexagonal and orthorhombic MoO_3 nanoparticles, J. Alloys Compd. 509 (2011) 8105, 10.

[19] H. Chuai, D. Zhou, X. Zhu, Z. Li, W. Huang, Characterization of V_2O_5/MoO_3 composite photocatalysts prepared via electrospinning and their photodegradation activity for dimethyl phthalate, Cuihua Xuebao/Chinese J. Catal. (2015).

[20] N. Danyliuk, T. Tatarchuk, K. Kannan, A. Shyichuk, Optimization of TiO_2-P25 photocatalyst dose and H_2O_2 concentration for advanced photo-oxidation using smartphone-based colorimetry, Water Sci. Technol. 84 (2021) 469–483.

[21] S.H. Elder, F.M. Cot, Y. Su, S.M. Heald, A.M. Tyryshkin, M.K. Bowman, Y. Gao, A. G. Joly, M.L. Balmer, A.C. Kolwaite, K.A. Magrini, D.M. Blake, The discovery and study of nanocrystalline TiO_2-(MoO_3) core-shelf materials, J. Am. Chem. Soc. 122 (2000) 5138–5146.

[22] Y. Takahashi, P. Ngaotrakanwiwat, T. Tatsuma, Energy storage TiO_2-MoO_3 photocatalysts, Electrochim. Acta 49 (2004) 2025–2029.

[23] H. Natori, K. Kobayashi, M. Takahashi, Fabrication and photocatalytic activity of TiO_2/MoO_3 particulate films, J. Oleo Sci. 58 (2009) 203–211.

[24] S. Bai, H. Liu, J. Sun, Y. Tian, S. Chen, J. Song, R. Luo, D. Li, A. Chen, C.C. Liu, Improvement of TiO $_2$ photocatalytic properties under visible light by WO_3/TiO_2 and MoO_3/TiO_2 composites, Appl. Surf. Sci. 338 (2015), 61–8.

[25] H. Liu, T. Lv, C. Zhu, Z. Zhu, Direct bandgap narrowing of TiO_2/MoO_3 heterostructure composites for enhanced solar-driven photocatalytic activity, Sol. Energy Mater. Sol. Cells 153 (2016) 1–8.

[26] X. Li, J. Xu, L. Mei, Z. Zhang, C. Cui, H. Liu, J. Ma, S. Dou, Electrospinning of crystalline MoO_3@C nanofibers for high-rate lithium storage, J. Mater. Chem. A 3 (2015) 3257–3260.

[27] W. Nuansing, S. Ninmuang, W. Jarernboon, S. Maensiri, S. Seraphin, Structural characterization and morphology of electrospun TiO_2 nanofibers, Mater. Sci. Eng. B 131 (2006) 147–155.
[28] I.M. Szilágyi, D. Nagy, Review on one-dimensional nanostructures prepared by electrospinning and atomic layer deposition, J. Phys. Conf. Ser. 559 (2014).
[29] K. Nakata, B. Liu, Y. Goto, T. Ochiai, M. Sakai, H. Sakai, T. Murakami, M. Abe, A. Fujishima, Visible light responsive electrospun TiO_2 fibers embedded with WO_3 nanoparticles, Chem. Lett. 40 (2011), 1161–2.
[30] N. Justh, G.J. Mikula, L.P. Bakos, B. Nagy, K. László, B. Parditka, Z. Erdélyi, V. Takáts, J. Mizsei, I.M. Szilágyi, Photocatalytic properties of TiO_2@polymer and TiO_2@carbon aerogel composites prepared by atomic layer deposition, Carbon N. Y 147 (2019) 476–482.
[31] O. Kéri, P. Bárdos, S. Boyadjiev, T. Igricz, Z.K. Nagy, I.M. Szilágyi, Thermal properties of electrospun polyvinylpyrrolidone/titanium tetraisopropoxide composite nanofibers, J. Therm. Anal. Calorim. (2019), 0.
[32] M.V. Someswararao, R.S. Dubey, P.S.V. Subbarao, S. Singh, Electrospinning process parameters dependent investigation of TiO_2 nanofibers, Results Phys. 11 (2018) 223–231.
[33] D. Hariharan, A. Jegatha Christy, J. Mayandi, L.C. Nehru, Visible light active photocatalyst: hydrothermal green synthesized TiO_2 NPs for degradation of picric acid, Mater. Lett. 222 (2018), 45–9.
[34] Y. Sun, J. Wang, B. Zhao, R. Cai, R. Ran, Z. Shao, Binder-free α-MoO_3 nanobelt electrode for lithium-ion batteries utilizing van der Waals forces for film formation and connection with current collector, J. Mater. Chem. A 1 (2013) 4736–4746.
[35] S. Alizadeh, S.A. Hassanzadeh-Tabrizi, MoO_3 fibers and belts: molten salt synthesis, characterization and optical properties, Ceram. Int. 41 (2015) 10839–10843.
[36] A. Chithambararaj, N.S. Sanjini, A.C. Bose, S. Velmathi, Flower-like hierarchical h-MoO_3: new findings of efficient visible light driven nano photocatalyst for methylene blue degradation, Catal. Sci. Technol. 3 (2013) 1405–1414.
[37] S. Kiennork, R. Nakhowong, R. Chueachot, Preparation and characterization of electrospun TiO_2 nanofibers via electrospinning preparation and characterization of electrospun, Integrated Ferroelectrics Int. J. 4587 (2015).
[38] A. Klinbumrung, T. Thongtem, S. Thongtem, Characterization of Orthorhombic α-MoO_3 Microplates Produced by a Microwave Plasma Process, 2012, 2012.
[39] S. Bagheri, K. Shameli, S.B. Abd Hamid, Synthesis and characterization of anatase titanium dioxide nanoparticles using egg white solution via Sol-Gel method, J. Chem. 2013 (2013).
[40] H. Zhang, M. Yu, X. Qin, Photocatalytic activity of TiO2 nanofibers: the surface crystalline phase matters, Nanomaterials 9 (2019) 535.
[41] J.Z. Ou, M.H. Yaacob, M. Breedon, H.D. Zheng, J.L. Campbell, K. Latham, Plessis J. Du, W. Wlodarski, K. Kalantar-zadeh, In Situ Raman spectroscopy of H_2 gas interaction with layered MoO3, Phys. Chem. Chem. Phys. 13 (2011) 7330.
[42] K.V. Karthik, C.V. Reddy, K.R. Reddy, R. Ravishankar, G. Sanjeev, R.V. Kulkarni, N. P. Shetti, A.V. Raghu, Barium titanate nanostructures for photocatalytic hydrogen generation and photodegradation of chemical pollutants, J. Mater. Sci. Mater. Electron. 30 (2019) 20646–20653.
[43] P. Intaphong, A. Phuruangrat, K. Karthik, P. Dumrongrojthanath, T. Thongtem, S. Thongtem, Effect of pH on phase, morphology and photocatalytic properties of BiOBr synthesized by hydrothermal method, J. Inorg. Organomet. Polym. Mater. 30 (2020) 714–721.
[44] A. Phuruangrat, P.O. Keereesaensuk, K. Karthik, P. Dumrongrojthanath, N. Ekthammathat, S. Thongtem, T. Thongtem, Synthesis of Ag/Bi_2MoO_6 nanocomposites using $NaBH_4$ as reducing agent for enhanced visible-light-driven photocatalysis of rhodamine B, J. Inorg. Organomet. Polym. Mater. 30 (2020), 322–9.